

Glassy dynamics in supercooled-liquid and glassy ethanol: A molecular dynamics study

M. A. González

Institut Laue Langevin, Boîte Postale 156, F-38042 Grenoble Cedex 9, France

E. Enciso

Departamento de Química Física I, Facultad de Ciencias Químicas, Universidad Complutense, Madrid E-28040, Spain

F. J. Bermejo

Consejo Superior de Investigaciones Científicas, Serrano 123, Madrid E-28006, Spain

M. Bée

Laboratoire de Spectrométrie Physique, UMR 5588, Université J. Fourier Grenoble-I, Domaine Universitaire, Boîte Postale 87, F-38402, Saint-Martin d'Hères Cédex, France

(Received 3 May 1999)

Static and dynamic properties of supercooled liquid and glassy ethanol are evaluated from computer molecular dynamics simulations and compared with experimental data whenever possible. In particular, a comparison with recent neutron-scattering data is done and the results indicate that the relatively simple model here employed is able to reproduce most of the observed features, at least on semiquantitative grounds. Special attention is paid to monitor how the relevant dynamical properties change through the glass transition region and to relate the phenomena observed with the microscopic information provided by the simulations.

I. INTRODUCTION

The understanding of the dynamics of supercooled liquids and glasses and whether or not the liquid-glass transition masks a subjacent thermodynamic phase transition still constitutes an open challenge to the condensed matter sciences.¹ Within the realm of idealized models, mode-coupling theory has constituted a significant advance towards our understanding of the origin of “glassy phenomena.”² However, a substantial theoretical effort still needs to be done to provide a molecular-scale version of the theory that could be applied unambiguously to real systems, although approaches to include in the theory the effects of molecular rotations have been developed recently.³

Apart from the canonical liquid→glass (LGT) transition, other transformations such as those involving the freezing of molecular rotations are known to share with it a good number of characteristics.⁸ Such freezing transitions are definitely pure dynamic in origin and therefore a comparison of the relevant phenomena associated with these and those shown by the LGT seems to constitute a promising route towards the clarification of the underlying physics behind these exceedingly interesting and pervasive phase transformations. Under such premises, a number of recent investigations have been recently carried out on a single system such as ethanol, as it allows us to study both transitions on the same material, which also take place under very close thermodynamic conditions. As known since two decades ago,⁴ this material exhibits an interesting polymorphism leading to phases that can be prepared depending upon temperature and cooling rates. The liquid can easily be supercooled and forms a topologically disordered solid (glass) if the temperature is decreased quickly below $T_g = 97$ K. If the glass is annealed at a temperature between 97 and 115 K or the cooling rate is

about 2 K/min it transforms into a plastic (or rotator-phase) crystal. Here, the molecules sit at the nodes of a bcc lattice, but they can rotate freely. The crystal undergoes upon cooling below ≈ 97 K an additional calorimetric (glass) transition, involving the freezing of molecules at random orientations. The resulting solid, which is referred to as an “orientational-glass,” shows no further transformation upon subsequent cooling. Alternatively, the stable, monoclinic orientationally ordered phase is easily prepared by annealing the liquid within the 120–158 K range.⁵

The orientational glass and the amorphous solid show surprising similarities in some macroscopic properties, such as the specific heat and the thermal conductivity. Their neutron-scattering spectra are also almost identical, and both show the characteristic excess “glassy” modes when compared with the stable crystal, suggesting that the dynamics of the disordered crystal phases of ethanol closely mimics that of the amorphous solid.⁶ Therefore, the possibility of studying in the same material both kinds of transition, one involving the arrest of all the degrees of freedom and another involving only the orientational ones, makes ethanol an ideal benchmark to deepen into the origin of this phenomenon.

Recently, Bermejo and co-workers have studied extensively all the phases of ethanol by means of neutron diffraction, inelastic neutron scattering, calorimetry, Raman, and dielectric spectroscopy.^{5–8} A series of molecular-dynamics (MD) simulations have also been performed to provide some complement to the experimental studies. Our goal here is twofold: first, to study in some detail the supercooled-liquid region, which is not easily accessible experimentally over long periods of time (many hours or days) due to the rapid formation of the ordered phases (monoclinic or plastic crystal) in this range of temperatures (110–159 K); second, we also aim to obtain a microscopic description of the different

motions that take place in the supercooled liquid and the glass, as well as in the crystalline phases, in order to use that information as an aid to analyze the experimental data and try to determine the importance of the different contributions (molecular translations and/or rotations) to the measured spectra.

In the present paper we analyze in detail the structure and dynamics of supercooled liquid and glassy ethanol and how they change near the liquid-glass transition region, while in a future paper we will report a comparative study of the dynamics in the different phases (glass, plastic crystal, and monoclinic crystal).⁹

Molecular simulations have often been used to study the behavior of supercooled liquids and glasses, going from hard sphere or Lennard-Jones systems¹⁰ to molecular liquids. In particular, methanol has been widely investigated by means of computer simulations^{11–13} and therefore our results can also be used to establish a comparison between the dynamics of an almost-rigid molecule such as methanol (characteristic frequencies are far too high to be relevant at the temperatures of interest) and that of a system that has one internal (molecular) degree of freedom, which has a frequency enabling mode hybridization with the “lattice” motions. It is suspected that the presence of this internal mode that leads to the appearance in the stable crystal of two molecular conformers in a 50:50 proportion is the main reason for the appearance of an stable plastic phase in the case of ethanol.

In summary, we aim to use the simulations as a tool helping with the analysis of experimental data whenever possible, in the search for microscopic evidences of the mechanisms underlying the different observed relaxations.

II. COMPUTATIONAL DETAILS

Although fairly detailed representations of the molecular interactions are nowadays possible on a system such as ethanol ($\text{CH}_3\text{CH}_2\text{OH}$), the phenomena under study are characterized by diverging relaxation times as one approaches the LGT and therefore a compromise between achievable simulation lengths and microscopic detail has to be made. Consequently, we have chosen the optimized potentials for liquid simulations (OPLS) potential,¹⁴ which being relatively simple has proven to give good results for the static and dynamic properties of normal-liquid ethanol.^{14–16}

This model considers the ethanol molecule as “semiflexible,” being the internal rotation along the axis C-O that gives rise to the *trans* and *gauche* isomers the only internal degree of freedom conserved. Forces are experienced by the model on four interaction sites, which are located on the CH_3 , CH_2 , O, and hydroxyl H groups. Interactions take the usual Lennard-Jones (LJ) form and electrostatic interactions are modeled by a set of point charges.¹⁴ The potential corresponding to internal rotation about the C-O bond is represented by means of a Fourier series with coefficients resulting in *trans-gauche* energy differences in reasonable agreement with experimental data (see Ref. 14 for details).

The simulation box contains 216 molecules under periodic boundary conditions. The initial configurations were obtained from a constant pressure ($P=0.8$ kbar) run using a cooling rate¹⁷ $dT/dt \approx 0.1$ K/ps. Subsequently, long runs for 12 different temperatures were performed in the microca-

nonical ensemble (constant NVE) to avoid the interference of the dynamics of the pressure bath with the particle dynamics and to facilitate the analysis of the data.¹⁸ The pressure was found to be fairly stable about the initial value of 0.8 kbar.

In both types of runs (NVE and NPT) the equations of motion were integrated using the Verlet leap-frog algorithm¹⁹ with a time step of 2.5 fs and bond lengths and angles were constrained by means of the SHAKE algorithm.²⁰ The interparticle interactions were truncated using a cutoff $R_c = 12.5$ Å and a switch function to avoid energy drifts.²¹ The chosen form was that described by Alonso *et al.*¹² That switch function turns off smoothly all the interactions between pairs of molecules whose center-of-mass separation is greater than the cutoff distance, enabling the total energy to be conserved.¹²

Standard corrections were applied to pressure and energy for the cutoff of the LJ interactions;¹⁹ whereas the electrostatics were treated by means of the reaction field technique using a constant $\epsilon_{\text{rf}}=25$, which is close to the value of the static dielectric constant of the material at ambient temperature.²³ This method gives equivalent results to those obtained when using the Ewald sums, at least for the calculation of the properties of interest here.^{16,22}

III. RESULTS

A. Thermodynamics and structure

The twelve thermodynamic states investigated and the main results obtained are summarized in Table I. The NVE energies agree with those calculated during the quench and are shown in Fig. 1, and, at comparable temperatures that are also in agreement with previous data.¹⁵ In Fig. 1 the temperature dependence of the density is also shown, together with experimental data for the liquid.²⁴ The OPLS model gives systematically low densities at ambient conditions ($\approx 3\%$),¹⁴ but at the isobar studied here ($P=0.8$ kbar) the calculated density is slightly higher than experiment at ambient pressure. As in the case of methanol, the model potential underestimates the thermal expansion coefficient, and this makes experimental and computed densities to coincide at the melting point of the stable crystal, $T_m = 159$ K (see Fig. 1).

The density and potential energy display a broad transition centered at about 150 K. The change in slope unveils the falling out of equilibrium, and the temperature where such a change appears is usually assigned as the computer glass-transition-temperature, T_g . Here, the calculated T_g comes about 53 K above experiment, a behavior previously found for methanol,¹¹ where $T_g(\text{exp})=103$ K versus $T_g(\text{MD}) \approx 155$ K. This is attributable to the high cooling rate employed in a simulation, which is several orders of magnitude higher than that of calorimetric measurements from where T_g is defined. The change in the V - T curve appears when the time scale of the molecular motions involved in the volumic relaxation following a decrease in temperature becomes of the same order than the observation time scale. Higher cooling rates mean that ergodicity is lost in a much shorter time scale and this leads to a transition that appears at temperatures well in excess of those where experiments are carried using achievable cooling rates, and also stretches over a wider range of temperatures.²⁵ However, the change in expansivity through the glass transition becomes quite within

TABLE I. Simulated state points and results. T is the average temperature of the run in K, ρ the density of the system in g/cm^3 , P the average pressure in kbar, t_{equil} and t_{sim} the equilibration and production times, respectively, in ps, E_{inter} the intermolecular potential energy in kJ/mol , U the potential energy including intramolecular, i.e., torsional, contributions in kJ/mol , $\%_{\text{trans}}$ the percentage of *trans* conformers, and D the self-diffusion coefficient in m^2/s . The latter have been obtained from the long-time slope of the mean-square displacement of the centers-of-mass. Below 160 K, they start to deviate from the Vogel-Tamman-Fulcher behavior observed at higher temperatures, thus indicating the transition to the nonergodic regime (see Fig. 7).

T	ρ	P	t_{equil}	t_{sim}	E_{inter}	U	$\%_{\text{trans}}$	D
298.6	0.810	0.83	100	246	-40.9	-38.9	50.2	9.6×10^{-10}
256.3	0.835	0.79	300	492	-43.4	-41.5	53.5	3.4×10^{-10}
216.5	0.861	0.74	500	819	-45.6	-43.8	57.1	8.3×10^{-11}
188.0	0.888	0.99	1000	1638	-47.1	-45.5	59.3	1.4×10^{-11}
160.0	0.901	0.82	1600	1638	-48.4	-47.0	64.8	$\approx 9.8 \times 10^{-13}$
142.6	0.911	0.83	3500	1638	-49.0	-47.6	65.4	$\approx 1.2 \times 10^{-12}$
123.6	0.918	0.71	3500	1638	-49.6	-48.3	68.0	$\approx 3.3 \times 10^{-13}$
104.4	0.932	0.98	3500	1638	-50.3	-49.0	66.8	$\approx 1.7 \times 10^{-13}$
85.4	0.941	0.96	5000	1638	-50.9	-49.6	66.1	$\approx 1.4 \times 10^{-13}$
61.1	0.948	0.85	3500	1638	-51.6	-50.4	66.8	≈ 0
41.5	0.955	0.84	2600	1638	-52.1	-51.0	66.8	≈ 0
5.9	0.965	0.82	2600	1638	-53.1	-52.0	66.2	≈ 0

the range of that measured by experiment. Thus, above 160 K we obtain a thermal-expansion coefficient $\alpha \approx 8 \times 10^{-4} \text{ K}^{-1}$, which compares well with typical values for liquid ethanol,²⁶ while below 140 K, $\alpha \approx 3 \times 10^{-4} \text{ K}^{-1}$, reasonably close to the experimental value obtained for the glass from recent neutron-diffraction measurements.²⁷ In other words, having the proviso about the validity of the simulation at these temperatures in mind, one sees that one of the most clear signatures of a glass transition is nicely mimicked by the calculation.

Previous studies have shown that the total radial distribution function for the normal liquid calculated using the OPLS model is in good agreement with experimental x-ray and

neutron-diffraction data.^{15,16} In Fig. 2 the intermolecular part of the function $D(r)$ is plotted for both the liquid and glass and compared with the experimental data obtained by Bermejo *et al.*⁵ This function is defined as

$$D(r) = 4\pi\rho r [g(r) - 1] = \frac{2}{\pi} \int Q [S(Q) - 1] \sin(Qr) dQ, \quad (1)$$

so it is directly related to both the calculated total $g(r)$ (computed as indicated in Ref. 16) and the measured structure factor $S(Q)$, therefore allowing us to compare between them. The figure shows the high resemblance between the structures of liquid and glass and the ability of the model to reproduce the structural data of the glassy state as well as for the liquid. The only significant differences between simulation and experiment occur in the region between 1.5 and 3 Å, but the errors in the experimental function in this region make useless any comparison. These errors are due to the inherent difficulty of subtracting the intramolecular part from the experimental data, as it can be checked by the large value obtained for the density from the initial slope of the experimental curve. At distances beyond 3–4 Å, the intramolecular contribution is much less important and one finds that the model accounts for the oscillations of the experimental $D(r)$, matching the positions of the maxima and minima, as well as their amplitudes.

The temperature dependence of the partial radial distribution functions below 160 K follows the same trends observed at higher temperatures in previous studies.¹⁵ On cooling the system, the first and second peaks increase and narrow, but the position of the first maximum does not change much with temperature. This indicates that the slower motion of the molecules makes the nearest- and next-nearest-neighbor shells become better defined. For temperatures below ≈ 100 K small extra peaks develop in the OO and OH partial correlation functions beyond the second-neighbor peak, at distances around 5–8 Å, which are associated with the increas-

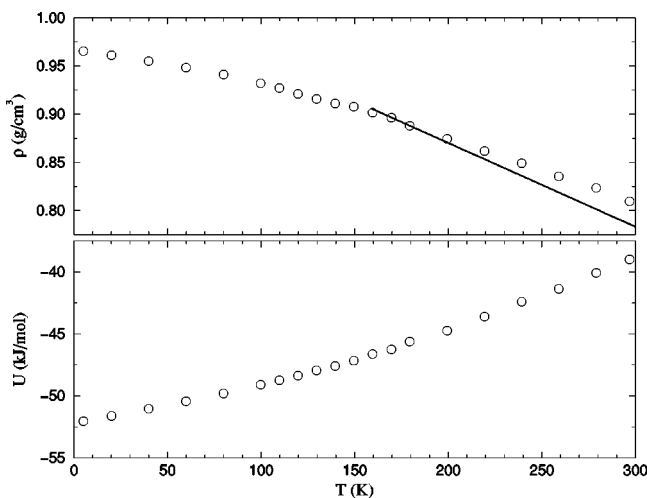


FIG. 1. Temperature dependence of the density (up) and the potential energy (down) obtained during the *NPT* quenching run. The solid line corresponds to experimental data for the density. (Ref. 24) The change of slope in the density and the potential energy at around 150 K marks the transition from the ergodic to the nonergodic regime, thus being this the corresponding T_g for the model and conditions employed in our simulations.

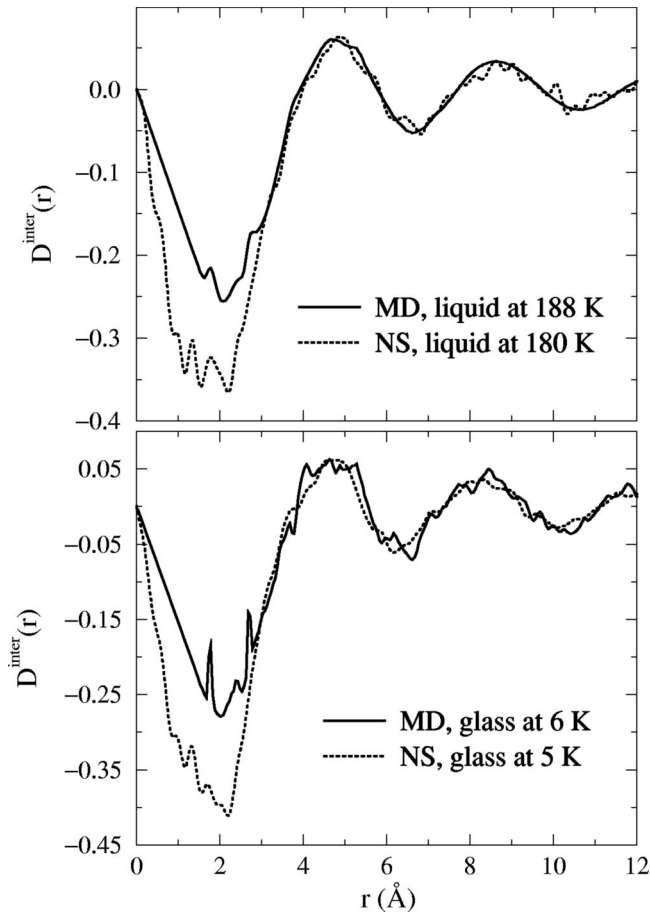


FIG. 2. Intermolecular radial distribution function, $D^{\text{inter}}(r)$, for liquid (up) and glassy (down) ethanol: comparison of simulation (solid lines) and experiment (dotted lines).

ing intermediate-range order. They appear close to the peaks observed in the $g(r)$'s of the monoclinic crystal, which is formed by infinite parallel chains of hydrogen-bonded molecules,²⁸ pointing to the close similarity of the local structure in both phases. This is shown in Fig. 3, where the radial distribution function for the centers of mass of the stable crystal⁹ is plotted and compared with that of liquid and glass. The first peak observed in the liquid corresponds to an envelope over the first series of four distinct peaks seen in the crystal. When cooling the liquid, the chains become longer and the molecular motion slower, so giving a more-defined structure than below 100 K, when the liquid is frozen into an arrested structure, it shows clear similarities at short distances with that of the crystal. Thus, the first peak of the monoclinic crystal at 3.7 Å appears as a shoulder in the $g_{\text{CM}}(r)$ of the glass at 100 K and as a distinct peak at 41 K; while the broad peak observed in the liquid seems to break into several peaks in the glass, which look like the remnants of the crystalline peaks located between 4.5 and 6.5 Å.

The absence of long-range order is apparent from the reduced amplitude of the second peak in both the atomic and center-of-mass radial distributions, and the correlations between molecules have disappeared almost completely for $r > 13\text{--}15$ Å, even in the case of the glass at the lowest temperature, which is in good agreement with the data obtained from neutron-diffraction measurements.⁵

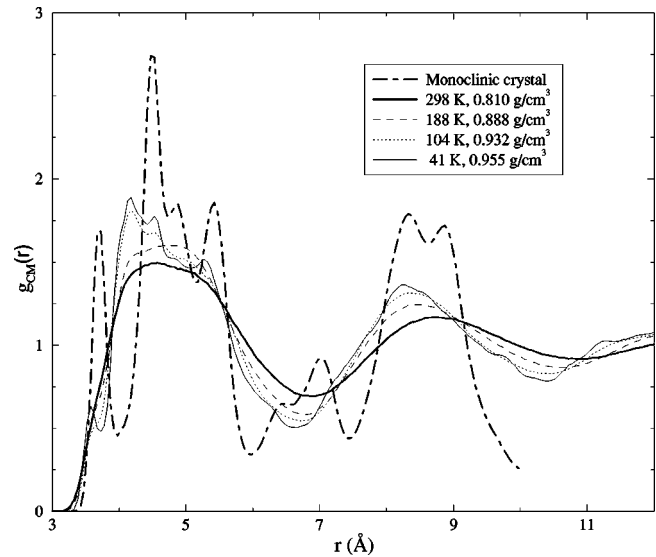


FIG. 3. Radial distribution functions for the centers of mass of liquid and glassy ethanol at 298 K (thick-solid line), 188 K (dashed line), 104 K (dotted line), and 41 K (thin-solid line). The function corresponding to the monoclinic crystal at 80 K is shown as a thick-dash-dotted line.

The degree of orientational order is quantified by means of the correlation function:

$$G_1(r) = \langle P_1[\cos \theta(r)] \rangle = \langle \cos \theta(r) \rangle, \quad (2)$$

where P_1 is the first Legendre polynomial and $\theta(r)$ the angle between the reference vector of two molecules whose centers of mass are separated by a distance r . In Fig. 4(a) the angular correlation of the molecular dipole moments at three different temperatures is shown. The results obtained using the OH bond as reference vector are very similar. One finds that only at short distances, $r < 5$ Å, i.e., those corresponding to the first-neighbor shell, there are clear correlations and $G_1(r) > 0$. Such correlations are lost for larger distances where $G_1(r)$ is close to 0, indicating that the molecules are randomly oriented. The interesting point to remark concerns the comparable extents of such orientational correlations with those found for the orientational-glass and plastic-crystal phases. In much the same vein, no large changes in $G_1(r)$ are observed with decreasing temperature, exception made of the emergence of some additional structure below 61 K arising from the freezing of the rotational motions.

In order to determine the influence of hydrogen bonding in the degree of orientational order, we have calculated $G_1(r)$ separately for molecules that are in the same H-bond chain and molecules that belong to different chains or clusters (see Sec. III C for details about the definition of an H bond and the H-bond structure). They are plotted in Fig. 4(b), together with the total function at room temperature. It is clear that the positive part of $G_1(r)$ at short distances comes from neighboring molecules that fulfil the geometric constraints associated with the presence of an H bond, while molecules belonging to different clusters or not directly H-bonded are randomly oriented giving $G_1(r)$ close to zero.

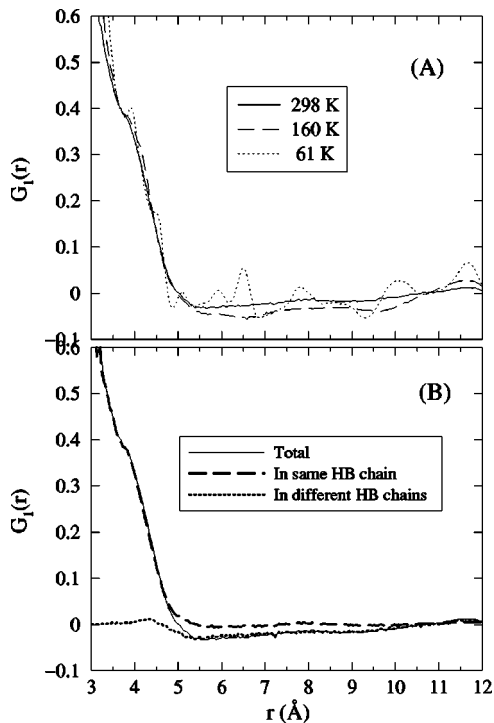


FIG. 4. (a) Orientational correlation function at 298 K (solid line), 160 K (dashed line), and 60 K (dotted line). (b) Orientational correlation function at room temperature (solid line) and contributions from molecules belonging to the same H-bond chain (thick-dashed line) and molecules belonging to different chains (thick-dotted line).

B. Internal rotations

Ethanol has one *trans* and two mirror-image *gauche* conformers, being the *trans* isomer the most stable in the gas phase.^{7,14} They are originated by the internal low-frequency motion along the C-O axis and seem to act as a source of frustration that increases the glass-forming ability of ethanol as compared to methanol.⁵ Thus, it is interesting to check how the ratio of isomers varies with temperature.

Integrating the average distribution of torsional angles between 120° and 240° the percentage of molecules in the *trans* state at each temperature was calculated and the results given in Table I. At high temperatures such distribution resembles that of the ideal gas;^{14,15} the percentage of *gauche* conformers is slightly higher in the liquid and with decreasing temperatures the difference between the percentage of *gauche* molecules in liquid and gas increases strongly. Our data also indicate that the number of *gauche* conformers present in the liquid below 100 K keeps roughly constant around a value of 33%. This is understandable as a result of the increasing density because of the more compact *gauche* form. It must be noted that the analysis of diffraction data indicates that the percentage of *gauche* molecules in liquid and glass is even larger, around 75%, although the calculation of this quantity from diffraction measurements is quite difficult and subjected to large errors.⁵

The dynamics of the internal rotation has been analyzed by means of the following autocorrelation function:¹⁵

$$C^A(t) = \frac{\langle c_i^A(t)c_i^A(0) \rangle}{\langle [c_i^A(0)]^2 \rangle}, \quad (3)$$

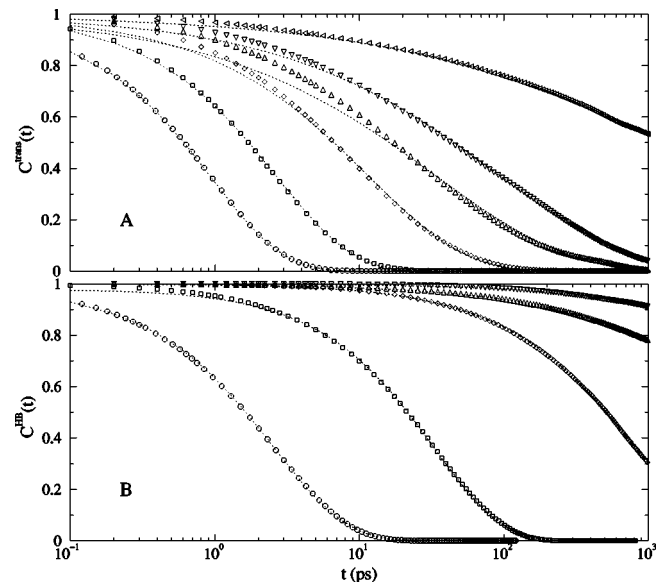


FIG. 5. (a) Autocorrelation function for the *trans* conformer at 298 K (circles), 216 K (squares), 160 K (diamonds), 124 K (triangles), 104 K (down triangles), and 61 K (left triangles) K. The dotted lines correspond to the KWW fits (see text). (b) Analogous results for the autocorrelation function of hydrogen bonds.

where $c_i^A(t)$ is equal to 1 if the molecule remains in the *A* state [$A = t, g_+ (0-120^\circ)$ or $g_- (240-360^\circ)$] along all the time interval going from time 0 to time t , and equal to 0 otherwise. A set of results are plotted in Fig. 5(a). We have also calculated the same function using the positions averaged over a time interval of 1.2 ps, in order to avoid considering those instantaneous jumps that are followed by an immediate return to the original state, and the resulting $C^A(t)$ is similar to the previous one in shape, but it falls down to zero more slowly. With decreasing temperature, the reduced kinetic energy available and the increased density hinder this internal motion and, as expected, the decay with time of $C^A(t)$ slows down; but even below T_g jumps between different conformers persist as indicated by the clear falloff of $C^A(t)$ at 61 K. $C^A(t)$ could not be fitted in the whole time range by a single exponential function, specially at low temperatures, so we used instead the Kohlrausch-Williams-Watts (KWW) law, which is often used as an empirical recipe to fit experimental data on supercooled liquids:²⁵

$$C^A(t) = A \exp[(-t/\tau_r^A)^\beta]. \quad (4)$$

The fits [shown as dotted lines in Fig. 5(a)] reproduce quite well the calculated function at long times, although for temperatures below 160 K some discrepancies appear at short times, a failure shared with studies on dielectric relaxation on different supercooled liquids.²⁹

The fact that a single exponential cannot fit $C^A(t)$ in the whole time range can be considered as an indication of the influence of the local environment into the dynamics of this internal motion, i.e., of the coupling between intramolecular and intermolecular modes, as if that motion were purely intramolecular, one would expect an exponential relaxation.

The relaxation times obtained for each kind of conformer using the instantaneous and averaged positions are given in Table II. As a consequence of the greater stability of the

TABLE II. Relaxation times of *trans* and *gauche* isomers and hydrogen-bond lifetimes in ps. The values given between parenthesis have been obtained using the averaged positions (see text).

$T(K)$	τ_r^{trans}	τ_r^{g+}	τ_r^{g-}	τ_r^{HB}
298.6	$9.5 \times 10^{-1} (2.9 \times 10^0)$	$8.6 \times 10^{-1} (2.0 \times 10^0)$	$8.4 \times 10^{-1} (2.0 \times 10^0)$	$2.6 \times 10^0 (3.0 \times 10^1)$
216.5	$2.7 \times 10^0 (7.5 \times 10^0)$	$2.1 \times 10^0 (4.4 \times 10^0)$	$2.1 \times 10^0 (4.5 \times 10^0)$	$3.3 \times 10^1 (4.8 \times 10^2)$
160.0	$1.2 \times 10^1 (4.3 \times 10^1)$	$7.7 \times 10^0 (1.9 \times 10^1)$	$7.7 \times 10^0 (1.8 \times 10^1)$	$8.0 \times 10^2 (\approx 2 \times 10^4)$
123.6	$3.5 \times 10^1 (1.6 \times 10^2)$	$2.3 \times 10^1 (5.3 \times 10^1)$	$2.3 \times 10^1 (6.7 \times 10^1)$	$\approx 1 \times 10^4 (\approx 3 \times 10^5)$
104.4	$9.6 \times 10^1 (4.3 \times 10^2)$	$6.2 \times 10^1 (2.2 \times 10^2)$	$6.1 \times 10^1 (1.9 \times 10^2)$	$\approx 3 \times 10^4 (\approx 1 \times 10^6)$
61.4	$\approx 3 \times 10^3 (\approx 1 \times 10^4)$	$\approx 1 \times 10^3 (\approx 2 \times 10^4)$	$\approx 2 \times 10^3 (\approx 1 \times 10^4)$	–

trans isomer, its relaxation times are longer than those of the *gauche* form at all temperatures. As for the latter, “ g_+ ” and “ g_- ” are mirror images and therefore they should show the same behavior. Thus, the differences between the different relaxation times obtained for each of them serve as an estimation of the statistical errors incurred in the calculation of $C^A(t)$, which are important for temperatures below ≈ 125 K, when the relaxation times become of the same order than that of the length of the simulation and the function is not available over a time range long enough to characterize clearly its decay and obtain reliable data from the fits.

C. Hydrogen bonds

The definition of a hydrogen bond involves geometric and/or energy criteria although both definitions lead to similar results.¹⁶ Thus, as in previous works,^{11,15,30} we consider that two ethanol molecules are H-bonded if $r(\text{O} \cdots \text{H}) \leq 2.6 \text{ \AA}$, $r(\text{O} \cdots \text{O}) \leq 3.5 \text{ \AA}$, and the angle $(\text{HO} \cdots \text{O}) \leq 30^\circ$.

The number of H bonds per molecule as a function of temperature as well as the fractions of molecules with 0, 1, 2, or 3 H bonds are given in Table III. As expected, such a number of H bonds increases with decreasing temperature. It is about 1.88 at room temperature, in agreement with x-ray data.³¹

Experiment and simulation data have been interpreted in terms of the existence in the liquid of winding chains^{31,32,14,15} or hexamer clusters.³³ The analysis of the simulation data shows that at 298 K linear chains are predominant. Closed

clusters of H-bonded molecules are found, but the number of molecules they contain is just a small fraction of the total number of molecules and hexamers are not specially abundant among them. At lower temperatures, the number of completely linear chains decreases and one finds that most of the chains found are partially closed over themselves through branching points formed by molecules with three H bonds. At the same time, the relative number of closed clusters increases and below 160 K, between 14 and 18% of the molecules are found in this kind of configurations. These clusters are typically small, as they are usually formed by a number of molecules between 4 and 7, although some larger clusters exist. In any case, we have not found any predominance of the hexameric form.

The data given in Table III confirm these observations. At the two highest temperatures the relatively high values of f_1 and f_3 (which are the percentage of molecules with 1 and 3 H bonds, respectively) indicate that the H-bond chains are short and “ramified.” When cooling, the chains become longer and the number of closed clusters increases, so the number of “end-molecules” f_1 strongly diminishes. At the same time, the number of “free” molecules falls down dramatically and below 100 K all of them become H-bonded, making $f_0=0$. At the lowest temperatures, the number of molecules with 1, 2, or 3 H bonds is basically constant, suggesting that tear and repair of H bonds has stopped or happens in time scales much longer than those accessible by the present simulations.

Representative results are shown in Fig. 6, where the number of chains per configuration is given for several temperatures as a function of the number of molecules they contain, n_m . At 298 K, there is a predominance of short chains and their number seems to decrease more or less in an exponential way with increasing length, which is characteristic of randomly bonded molecules.¹⁵ With decreasing temperature, the distribution loses its exponential character and below 200 K there is already a significant number of long chains. For temperatures about 160 K and below, freezing of the H-bond structure is almost complete. Nevertheless, by following the behavior of the individual chains it is possible to check that even at 100 K some molecular mobility persists and, especially at the ends or the branching points of the chains, some molecules can perform high amplitude motions that lead to a local rearrangement of the chains. Anyway, this kind of motion seldom occurs below 160 K so that it has almost no influence in the relaxations observed, as it would be necessary to perform simulations spanning several more decades

TABLE III. Number of hydrogen bonds and percentage of molecules with 0, 1, 2, or 3 H bonds. Below 61 K no changes are observed and the distribution of molecules with different number of H bonds is exactly the same than at 61 K.

$T(K)$	n_{HB}	f_0	f_1	f_2	f_3
298.6	1.88	1.3	14.6	78.5	5.6
256.3	1.96	0.3	8.4	86.4	4.8
216.5	1.99	0.1	4.7	91.7	3.6
188.0	2.00	<0.1	3.1	94.1	2.8
160.0	2.00	<0.1	1.6	96.9	1.5
142.6	2.00	<0.1	2.8	94.4	2.8
123.6	2.00	<0.1	3.2	93.5	3.2
104.4	2.00	0.0	2.3	95.4	2.3
85.4	2.00	0.0	2.9	94.3	2.9
61.1	2.00	0.0	2.8	94.4	2.8

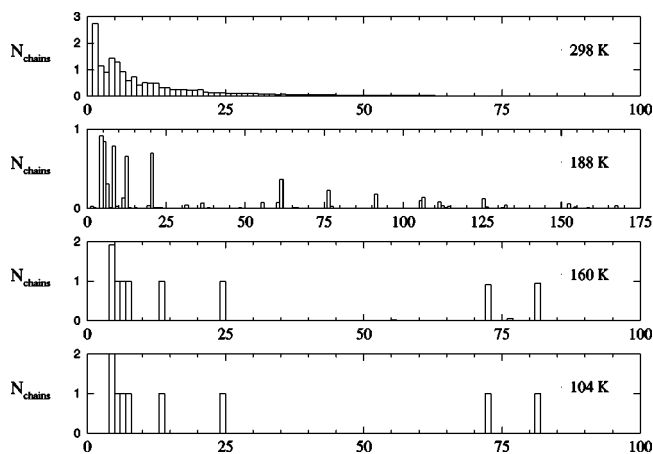


FIG. 6. Hydrogen-bond histogram showing the average number of chains with n_m molecules at four different temperatures. Below 104 K no changes are appreciated in the distribution of chains in the time window corresponding to our simulations.

in time in order to appreciate the dynamic effects brought forward by these kinds of jumps.

An activation energy for the formation or breaking of an H bond is obtained from data for f_0 in the liquid side ($1000/T < 6.25$). It yields 21.0 kJ/mol, which compares with 16.7 kJ/mol for methanol.¹¹

Our estimation of 21 kJ/mol is in reasonable agreement with NMR data on supercritical ethanol³⁴ if a model involving cluster distributions³⁵ is used to analyze the data instead of the simple two-state model employed in the original paper.

The lifetime of the H bonds was calculated by means of³⁶

$$C^{\text{HB}}(t) = \frac{\langle \eta_{ij}(t) \eta_{ij}(0) \rangle}{\langle [\eta_{ij}(0)]^2 \rangle}, \quad (5)$$

where $\eta_{ij}(t)$ is equal to 1 if molecules i and j have been H-bonded uninterruptedly between time 0 and time t and 0 otherwise. This autocorrelation function is similar to that employed to calculate the relaxation times of the *trans* and *gauche* conformers and, as before, we have used the instantaneous positions and the positions averaged over a time interval of 1.2 ps to compute it. This allows us to average out the high amplitude motions that cause the breakdown of a H-bond just for a very short time, but are followed by its immediate reforming. Figure 5(b) shows the autocorrelation functions obtained at several temperatures when using the instantaneous positions, while the curves obtained using the averaged positions have a similar shape, but decay much more slowly. As before, a KWW law fits the data quite well (the fits are shown as dotted lines in the figure) and allow us to estimate the average life of a H bond as a function of temperature. The results are given in Table II and show the rapid increase of the average lifetime of the H bonds with decreasing temperature. In fact, at 61 K we found that none of the H bonds existent in the initial configuration was broken in the time scale of the simulation.

It is interesting to note that in this case, the fits follow quite well the calculated curves even at short times, where the KWW law fails to describe $C^{\text{trans/gauche}}(t)$. This can be tentatively explained by considering that the short-time mo-

lecular relaxation is mainly of vibrational origin and cannot be accounted by the “stretched exponential” form. As the intermolecular vibrations have not enough amplitude to break the H bonds, they will not influence the decay of $C^{\text{HB}}(t)$, which can then be correctly described by the KWW law; while as they effectively couple with the internal torsional mode they can affect the initial decay of $C^{\text{trans/gauche}}(t)$, making the KWW equation fail at short times in this case.

D. Single-particle dynamics

1. Diffusion coefficient

At high temperatures, the mean-square displacement (m.s.d.) of the molecular centers of mass presents the characteristic diffusive behavior of simple liquids. With decreasing temperature the mobility of the molecules is dramatically reduced and the global diffusion is arrested at about 124 K, coinciding roughly with the temperature at which the H-bond configuration is frozen.

At very short times ($t < 0.5$ ps), the m.s.d. shows a quadratic dependence in time and a mild behavior with temperature. This regime is dominated by the collective vibrational dynamics. At longer times there is a transition to the characteristic diffusive regime of a liquid, which is strongly temperature dependent. In between, an intermediate subdiffusive regime appears, becoming increasingly extended with decreasing temperature. This intermediate region indicates that the molecules are vibrating within configurations of neighbors that are stable within scales of several hundreds of ps. Escape from that cage leading to long-range mass diffusion involves concerted molecular motions that make the cage configurations dynamically unstable. Finally, at even lower temperatures, the molecules have not enough energy to break the H bonds, so they are confined to vibrate inside their cage or librate around their H bonds and the m.s.d. does not increase with time after the initial fast regime.

The long-time slopes of the mean-square curves provide a measure of the self-diffusion coefficient D . The results are given in Table I and they are compared with experimental data³⁷ in Fig. 7. We have plotted the experimental data at atmospheric pressure and at $P = 1$ kbar, which show that the dependence of D with pressure is much smaller than the temperature dependence. The calculated coefficients agree quite well with the experimental data and follow the Vögel-Tamman-Fulcher (VTF) law used by Karger *et al.* to fit their NMR data.³⁷ Below 160 K, the data start to deviate from the VTF law, although the values of the self-diffusion coefficient are already so small that it is impractical to give a physical meaning to this fact and to their behavior below that temperature. The fact that this temperature matches that defined by the change in slope of the energy or the volume indicates that the thermodynamic and dynamic properties are being sampled in the same time scale.

In Fig. 8, the m.s.d. at several observation times is plotted as a function of temperature. For the smallest time (0.2 ps), $\langle \Delta r^2(t) \rangle$ follows the expected harmonic behavior up to room temperature, whereas deviations from it are observed at larger times. The departure from linearity occurs around 100 K, i.e., the calorimetric T_g . The same has been found in other computer-simulation studies and suggest the intimate

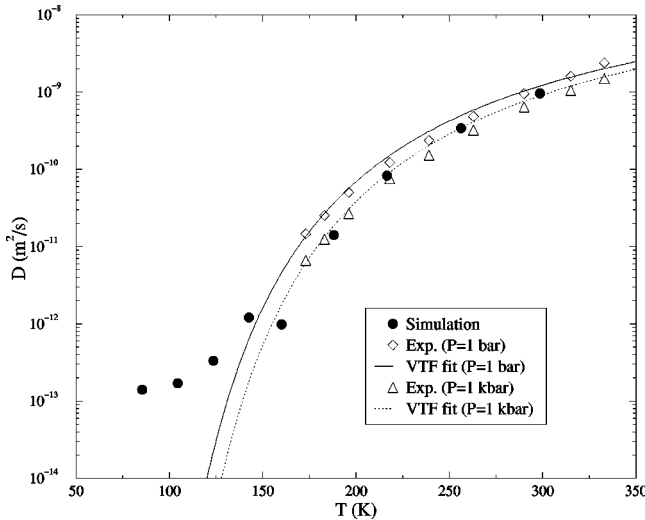


FIG. 7. Temperature dependence of the self-diffusion coefficient. Results from the MD simulation are shown as black circles and the open symbols correspond to experimental data at 1 bar (diamonds) and 1 kbar (triangles). The lines are VTF fits to the experimental data (Ref. 37). The departing of the simulated points from those experimental curves at the same temperature where the density or the energy change slope indicates that the transition to the nonergodic regime takes place at the same temperature for thermodynamic and dynamic properties, so confirming previous results on methanol that indicated that those were probed on the same time scale by the simulations (Ref. 11).

relation between the short-time dynamics and the phenomena observed on much longer time scales.²⁵ Those anharmonicities can be thought as a first sign or a precursor of the glass-to-liquid transition,^{25,38} which would take place when anharmonicity is large enough to get over the restoring forces that keep the mechanically stable arrangement corresponding to a particular minimum of the configuration space, so the system starts to explore other minima of that configuration space.³⁹

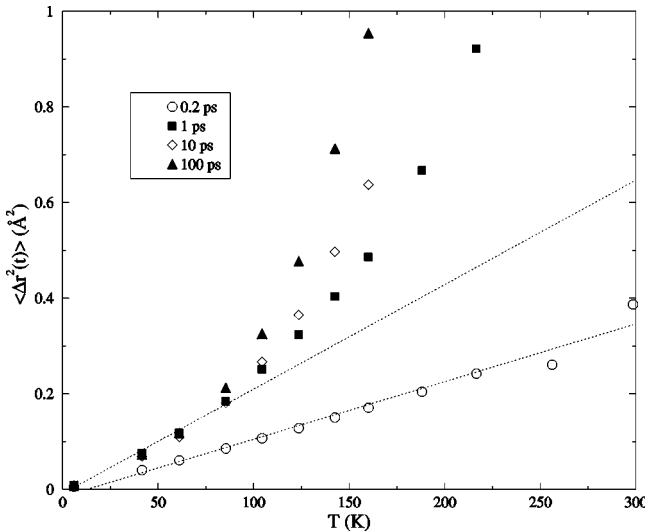


FIG. 8. Center-of-mass mean-squares displacements as a function of temperature for several observation times.

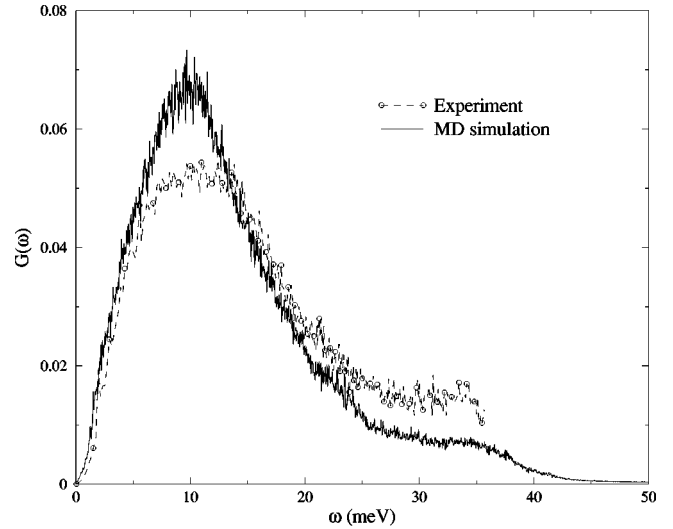


FIG. 9. Density of vibrational states of glassy ethanol. Comparison of simulation (solid line) and neutron-scattering data (dashed line with open circles).

2. Velocity autocorrelation functions and densities of vibrational states

The negative region in the velocity autocorrelation function (not shown) becomes more pronounced as the temperature is decreased. This indicates the stepwise freezing of all the degrees of freedom involving mass and rotational diffusion as the temperature is lowered. The Fourier transform of the velocity autocorrelation function gives the density of vibrational states (DOVS), $G(\omega)$, which is a property that can be obtained also from inelastic neutron-scattering experiments as

$$G(\omega) = \omega^2 \left[\frac{S_s(Q, \omega)}{Q^2} \right]_{Q \rightarrow 0}, \quad (6)$$

where $S_s(Q, \omega)$ is the self- (incoherent) dynamical structure factor measured experimentally for several wave vectors Q . The density of vibrational states of the glass given by the model is compared with experiment⁶ in Fig. 9. Some discrepancies exist concerning the intensity of the maximum and the decay of the DOVS for $\omega > 20$ meV, but the overall agreement is quite good considering the quasirigid nature of the model. The calculated curve also reproduces correctly the contribution of the lower-frequency modes ($\omega < 5$ meV), the position of the maximum and the width of the broadband observed experimentally.

3. Van Hove self-correlation functions

The self part of the density autocorrelation or Van Hove function is defined as

$$G_s(\mathbf{r}, t) = \frac{1}{N} \left\langle \sum_{i=1}^N \delta[\mathbf{r} - \{\mathbf{r}_i(t) - \mathbf{r}_i(0)\}] \right\rangle. \quad (7)$$

For an isotropic body, only the modulus of \mathbf{r} is relevant and after performing the angular integration one gets $4\pi r^2 G_s(r, t)$, which gives the probability that a particle has moved a distance r in a time interval t . In Fig. 10, we plot

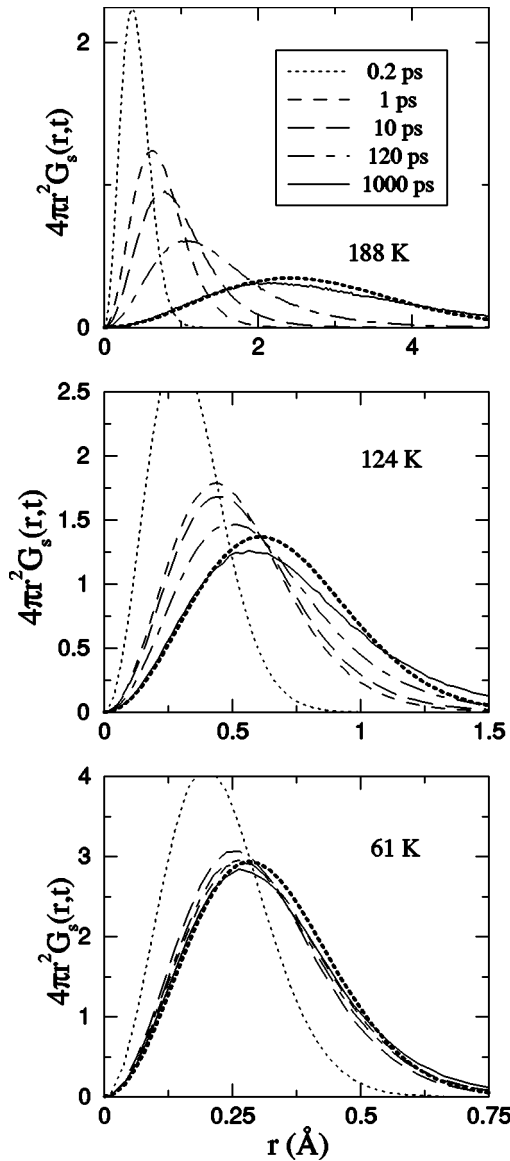


FIG. 10. Self-part of the Van Hove function at three different temperatures, 188 K (up), 124 K (medium), and 61 K (down) for the following observation times: $t = 0.2$ ps (dotted line), 1 ps (dashed line), 10 ps (long-dashed line), 120 ps (dash-dotted line), and 1000 ps (solid line). The thick-dotted line corresponds to the Gaussian approximation to $G_s(r, t = 1000$ ps) (see text).

that function for the molecular centers of mass at three temperatures. At 188 K [Fig. 10(a)], the curves corresponding to several times t have a single peak whose maximum moves to larger distances with increasing time, indicative of diffusive motion. Such peak shifts are nearly arrested at 124 K [Fig. 10(b)], i.e., about the temperature where the m.s.d. does not show any sign of mass diffusion. Anyway, the fact that the maximum of the function is still moving with time indicates that a molecule could move over a distance of the order of the first-neighbor separation, which is ≈ 4 Å (see Fig. 3), on a much longer time scale, which is outside of the time window of our simulations. Finally, at 61 K [Fig. 10(c)] there is no longer any trace of diffusive motion after the initial vibrational relaxation occurring at times less than 1 ps, so the sample is completely arrested. The atomic functions (not shown) are very similar to those corresponding to the mo-

lecular centers of mass, and neither of them present a double peak structure, which would indicate the existence of jump motions.⁴⁰

The non-Gaussian character of the density autocorrelation function can be best gauged comparing $G_s(r, t = 1000$ ps) with a Gaussian function fitted to short distances to it and plotted in Fig. 10 as a thick dotted line. The motion of the molecular centers of mass is again Gaussian at very short times only (free-particle motion) and at very long times, in the hydrodynamic limit (diffusive motion). In between, the coefficient of non-Gaussianity, $\alpha_2(t)$, shows a strong non-Gaussian behavior, which increases with decreasing temperature, extending over a longer-time interval. The same behavior is found in simulations of many other supercooled liquids.^{10,38}

4. Incoherent dynamical structure factor

The incoherent dynamical structure factor or self-intermediate scattering function is the time density-density correlation function for a tagged particle. In order to compare with experiment it has been calculated using the following equation:

$$F_s(\mathbf{Q}, t) = \frac{1}{N} \sum_i b_{i,inc}^2 \langle \exp[-i\mathbf{Q} \cdot \mathbf{r}_i(0)] \exp[i\mathbf{Q} \cdot \mathbf{r}_i(t)] \rangle, \quad (8)$$

where the sum runs over all the atoms and $b_{i,inc}$ are their incoherent scattering lengths. This is the spatial Fourier transform of $G_s(r, t)$ and gives direct information on relaxational processes. It can be Fourier transformed in order to give the dynamic structure factor $S_s(\mathbf{Q}, \omega)$, which is accessible experimentally by means of incoherent inelastic neutron scattering. This is done in Fig. 11(a), where the calculated and experimental⁵ dynamic structure factors are compared for the wave vector corresponding to the maximum of the static structure factor, i.e., $Q = 1.6$ Å⁻¹. In order to compare them, the simulated spectrum has been multiplied by the detailed balance factor, and both curves have been normalized to the same area. The calculated $S_s(\mathbf{Q}, \omega)$ has a Boson peak that is situated at a slightly lower frequency and is more prominent and decays somewhat faster than experiment, as it could be expected from the results obtained for $G(\omega)$, which is directly related to $S_s(\mathbf{Q}, \omega)$ [Eq. (6)]. Size-effects and the high-cooling rate employed, as well as possible deficiencies of the force field, are probably at the origin of those discrepancies, but at any rate, the simulation reproduces quite well the features observed by neutron spectroscopy, so the microscopic dynamics given by the model can be considered to be a reliable representation of the dynamics of real ethanol, at least at a qualitative level.

The center-of-mass intermediate-scattering function corresponding to the wave vector $Q = 1.6$ Å⁻¹ is plotted in a semilogarithmic scale in Fig. 12(a). There is an initial fast decay that is almost temperature-independent and corresponds to the vibrational relaxation. This happens for $t \lesssim 0.2$ ps, i.e., on a time scale typical of inverse phonon frequencies and is followed by the slow α or structural relaxation, which depends strongly on the temperature and becomes almost arrested for temperatures below 140 K.

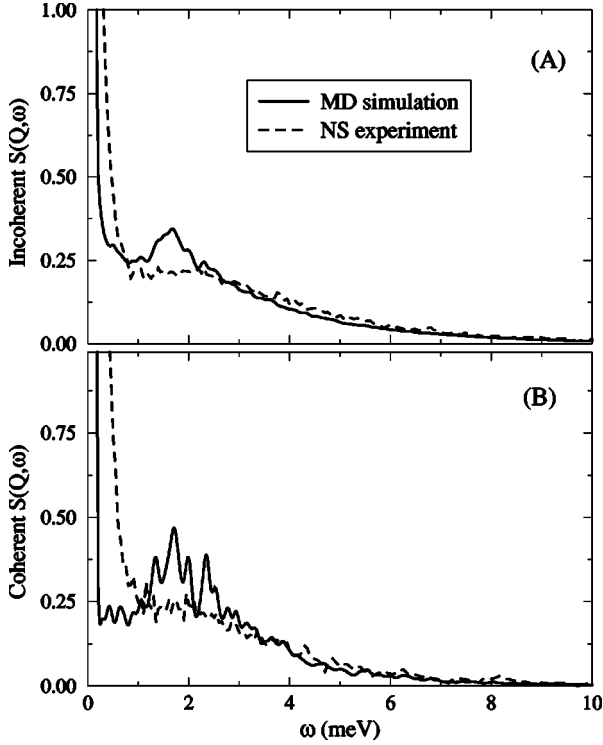


FIG. 11. Comparison of the experimental (dashed line) and computed (solid line) dynamic structure factor $S(Q, \omega)$ at $Q = 1.6 \text{ \AA}^{-1}$. (a) Incoherent part (hydrogenated sample in the inelastic neutron-scattering experiments). (b) Coherent part (deuterated sample).

An intermediate relaxation occurring on a time of several ps can be tentatively identified with the part of $F_s(Q, t)$ that shows a positive curvature, although the possible influence of size effects in this time region should be checked.⁴¹

The data between 5 ps and $t_{sim}/2$, where t_{sim} is the maximum length of each run, have been fitted to the KWW equation:

$$F_s^{CM}(Q, t) = A(Q) \exp[-(t/\tau)^\beta]. \quad (9)$$

The fits obtained [represented by dotted lines in Fig. 12(a)] are reasonably good, although the limitations in length of the simulations and the statistical noise of the calculated $F_s(Q, t)$ put some uncertainty in the fitted values, specially in those for $A(Q)$ at high temperatures and for β and τ at low temperatures. The relaxation times increase exponentially with decreasing temperature, as shown by the values given in Table IV for two different values of Q . Below 160 K, they become several orders of magnitude longer than the time window spanned by our simulations. Thus, at the lowest temperatures, runs are not long enough to allow for the complete relaxation of the system within the time of the simulation. With decreasing temperature, β goes from liquid-like values ($\beta=1$ in a simple liquid) to a value around 0.4 for $T < 150$ K. In agreement with the behavior of β or τ , the amplitude parameter or the so-called nonergodicity parameter $A(Q)$ is also roughly harmonic at low temperatures, departing from linearity afterwards.

These results show that, in agreement with the behavior observed for the self-diffusion coefficient, the translational

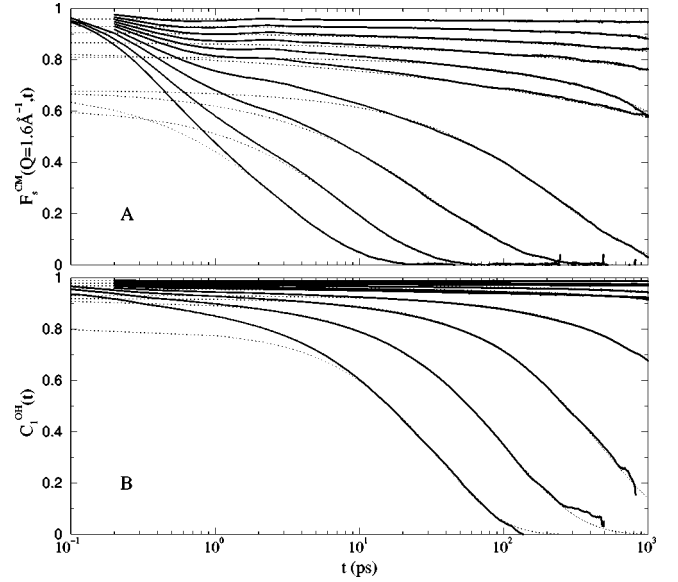


FIG. 12. (a) Self-intermediate scattering function for the wave vector $Q = 1.6 \text{ \AA}^{-1}$. From bottom to top, the solid curves correspond to the following temperatures: $T = 298, 256, 216, 188, 160, 143, 124, 104, 85,$ and 61 K. The dotted lines correspond to the KWW fits (see text). At high temperatures they decay to zero within the time scale of the simulation, while the transition from the ergodic to the nonergodic regime is clearly shown by the change of behavior of the curves around $140\text{--}160$ K. (b) Same for the reorientational correlation function $C_1^{OH}(t)$.

relaxation times diverge at a temperature around ≈ 150 K. Below that temperature, we are into the nonergodic regime and not all of the relaxation mechanisms present in the liquid are manifested now on the time scale of the simulation, so the properties obtained will depend on the particular configurational state in which the system has fallen during the quenching procedure. In this regime, a quantitative study of the relaxation mechanisms that continue to take place is out of reach, but the motions observed, such as small local atomic rearrangements and partial reorientations, can be used as clues of the kind of motions that persist in the glass.

5. Orientational relaxation

The rotational dynamics of the individual molecules is best specified by

$$C_l(t) = \langle P_l[\cos \theta(t)] \rangle, \quad (10)$$

where P_l is the l th Legendre polynomial and $\theta(t)$ is the angle swept by a reference vector of the molecule in the time t . The correlation times obtained using the 1st and the 2nd

TABLE IV. Characteristic translational and rotational relaxation times in ps.

$T(K)$	$\tau[F_s^{CM}(Q=0.8, t)]$	$\tau[F_s^{CM}(Q=1.6, t)]$	$\tau[C_1^{OH}(t)]$
298.6	1.3×10^1	2.9×10^0	3.6×10^1
256.3	3.5×10^1	8.4×10^0	1.0×10^2
216.5	1.6×10^2	3.3×10^1	4.8×10^2
188.0	$\approx 1 \times 10^4$	2.4×10^2	$\approx 5 \times 10^3$
160.0	$\approx 9 \times 10^5$	$\approx 4 \times 10^4$	$> 10^8$

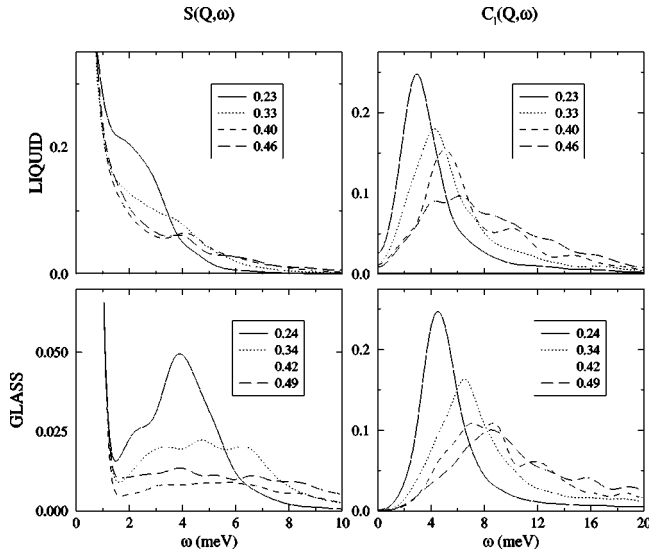


FIG. 13. Total dynamic structure factors, $S(Q, \omega)$ (left side) and the corresponding longitudinal current correlations (right) for liquid (up) and glass (down) for wave-vector values given as insets.

Legendre polynomials can be related to the times measured by dielectric relaxation and NMR experiments, respectively.⁴² For the liquid, the correlation times obtained with the OPLS model are significantly smaller than those found experimentally.^{15,16} Nevertheless, their temperature dependence is deemed reasonable.

In Fig. 12(b), $C_1^{\text{OH}}(t)$ is plotted. The other functions obtained using the OH and μ vectors as reference vectors and the 1st or 2nd Legendre polynomial are very similar in shape to that one. They all show an initial relaxation due to the librational motion of the molecules followed by the slow α relaxation and can also be fitted by a KWW law [dotted lines in Fig. 12(b)]. The correlation times obtained for the reorientation of the OH vector are given in Table IV. They behave as the relaxation times corresponding to the center-of-mass motion obtained before from the fits of $F_s^{\text{CM}}(Q, t)$, indicating that translational and rotational motions are coupled and slow down together with decreasing temperature.

E. Collective dynamics

The total intermediate scattering function $F^{\text{CM}}(Q, t)$ for the molecular centers-of-mass has also been evaluated and its time Fourier transforms, the dynamical structure factor $S(Q, \omega)$ are shown in Fig. 13. Well-defined (i.e., non-overdamped) inelastic peaks are seen for both liquid and glass for the lowest-explored wave vector (0.23 \AA^{-1}) only. As shown in Fig. 13, plotting the quantities $C_l(Q, \omega) = \omega^2 S(Q, \omega) / Q^2$ (i.e., the longitudinal current-current correlations) unveils that, apart from a lifetime effect that results on a homogenous broadening of the main peak, a significant part of the width of $C_l(Q, \omega)$ for larger wave vectors arises from the increasing contribution to the spectra from “modes” with frequencies well above those characteristic of the acoustic branches of the monoclinic crystal⁷ (i.e., well above $\approx 5 \text{ meV}$). Indeed, several subsidiary maxima can be

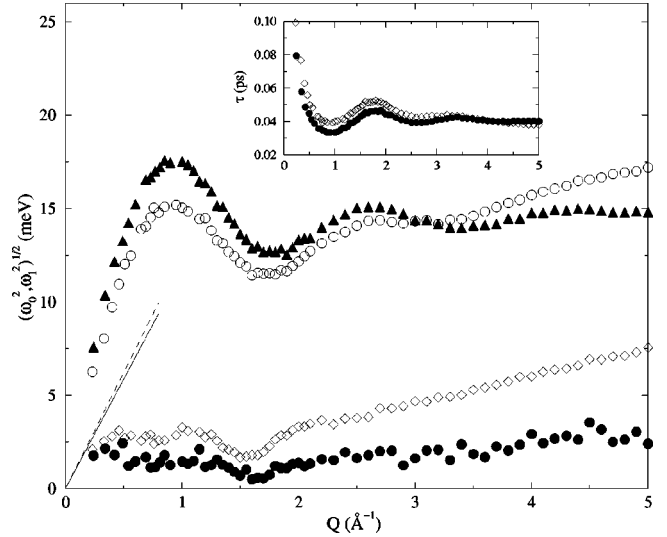


FIG. 14. Reduced-frequency moments, ω_0 and ω_l . Solid symbols (filled dots and triangles) correspond to ω_0 and ω_l for the glass and open symbols to liquid. The inset shows the relaxation time as evaluated in the viscoelastic approximation.

tracked down with increasing Q values, which on the basis of previous lattice dynamics results can be assigned to mostly “optic-like” motions.⁷

The important point to stress from the above considerations concerns the presence of a strong-scattering regime where only acoustic excitations with characteristic frequencies comparable or below that of the “Boson peak” can travel a distance larger than that corresponding to one molecular diameter. To quantify this, Fig. 14 shows the reduced frequency moments defined as $\langle \omega^n \rangle = \int d\omega \omega^n S(Q, \omega)$ that are calculated for both liquid and glass.⁴³ For an isotropic medium such as a liquid, $\lim_{Q \rightarrow 0} \omega_0^2 = Q^2 v_T^2$, with $\omega_0^2 = \langle \omega^2 \rangle / S(Q)$, provides an estimate of the isothermal velocity v_T , so that v_T can be derived from extrapolation to $Q \rightarrow 0$ of the phase velocity $c_{ph} = \omega_0 / Q$. In doing so, one obtains values of $\approx 1890 \text{ m/s}$ and $\approx 1780 \text{ m/s}$ for the glass and liquid, respectively. Using such values for v_T , one can draw the hydrodynamic dispersion laws $\omega_{hyd} = v_T Q$, which are also shown in Fig. 14. The point to remark here concerns the approach to hydrodynamics of both ω_0 moments for the glass and liquid “from below,” that is as expected for normal sound dispersion. On the other hand, the lifetime of a given excitation can be expressed under the viscoelastic approximation⁴³ as $\tau^{-1} = 2\sqrt{(\omega_l^2 - \omega_0^2)}/\pi$, with $\omega_l^2 = \langle \omega^4 \rangle / \langle \omega^2 \rangle$. From plots shown in Fig. 14 it is inferred that sound propagation is bounded to frequencies below 3 meV , and that the lifetimes of such excitations only reach values beyond 1 ps , that is those required to travel a mean-free path of a few molecular diameters, at scales well outside those reachable by the simulation.

The results are also in good agreement with experimental neutron work (see Fig. 11), which show that for wave vectors well above $Q \geq 0.25 \text{ \AA}^{-1}$ the peak at 2.6 meV known as the “Boson peak” is the only finite-frequency feature that appears superposed to a broad inelastic background. Its characteristic frequency is strikingly close to that of ω_0 for large wave vectors. The peak, clearly visible in $S_s(Q, \omega)$ at all explored Q values develops in the total $S(Q, \omega)$ for Q

$\geq 0.7 \text{ \AA}^{-1}$ only. This fact seems to point towards the multi-excitation (or Umklapp-scattering) nature of such a feature, since such processes are expected to show a dependence on Q^2 as well as upon an integral that involves the static structure factor,⁴⁴ which can lead to a narrow peak. Also, in agreement with recent neutron data measured at low temperatures (4 K) the peak, as shown in Fig. 11 becomes remarkably sharp,⁴⁵ its position shows no measurable dependence with Q , and its frequency is also very close to that of a similar feature appearing in the powder spectra of the monoclinic polycrystal.

IV. CONCLUSIONS

A comparison with available experimental data as detailed as possible, shows that a simple model developed for the liquid is able to reproduce most of the experimental observations for supercooled and glassy ethanol.

Such a model is able to mimic the real glass-transition as evidenced by the change in the slope of thermodynamic properties, such as the density or the potential energy. This takes place at about 150 K, which is considerably higher than the experimental T_g . We attribute this discrepancy to the high-cooling rate employed in the simulation. The dynamic properties studied also point to a transition to a nonergodic regime around that temperature. The relaxation times corresponding to different kind of motions (breaking of a H bond, translation, and reorientations) as obtained from KWW fits give indications of divergent behavior at temperatures below 160 K, which cannot be followed in detail at lower temperatures since they go outside our time window.

The self-diffusion coefficients (Fig. 7) also follow quite well the experimental VTF law corresponding to the liquid up to that temperature, while below they change erratically due to their small magnitude and the nonergodicity of this regime.

The progressive slowing down of the dynamics with decreasing temperature and the coupling of translational and reorientational motions can also be viewed as resulting from the increasing difficulty to break the H bonds, as can be gauged by comparing Figs. 5 and 12.

At 60 K and below, there is no further rearrangement of the H-bond network, at least in the time scale of ns explored here, and the quenched configuration is practically frozen. At intermediate temperatures, some molecular motions such as atomic or even molecular jumps and large molecular reorientations are observed. Although they are too scarce to contribute to the Van Hove self-correlation function, their contribution to the long-time decay of $F_s(Q, t)$ or $C_l(t)$ is apparent in Fig. 12, and these have been shown to be the

microscopic entities giving rise to relaxation at dielectric scales.⁸

The internal motion corresponding to the torsion along the C-O axis is not arrested at 60 K and their relaxation times show no sign of divergence. Its nonexponential character is probably an indication of the coupling of intramolecular and intermolecular modes. We have found that at low temperatures the observed molecular jumps or reorientations are normally associated with a jump between different isomers, which can be followed or not by a return to the previous conformer state. Thus, the torsional mode could act as an additional degree of freedom that serves to stabilize the new structural arrangement.

In summary, we have followed by means of MD simulations the ergodic–nonergodic transition in a simple model for ethanol that reproduces quite correctly the slowing down of the dynamics observed experimentally down to temperatures around 150 K (see Fig. 7). Below that temperature, the rapid cooling rate employed and the time window imposed by computational limitations determine the nature of the nonequilibrium state achieved and, therefore, the data obtained at the lowest temperatures do not correspond to a true glassy state of ethanol. This is a concomitant problem to any computer-simulation study of the glassy state, although nowadays simulations of several hundreds of ns have already been performed for supercooled water,⁴⁶ as the experimental relaxation times corresponding to the calorimetric glass transition temperature (≈ 100 s) are completely unattainable. Nevertheless, the reasonable agreement between the experimental and computed structures and dynamic spectra (Figs. 2, 9, and 11) indicates that the simulated glass reproduces qualitatively the main features observed experimentally, allowing us to obtain some clues about the microscopic motions that persist below T_g and accounting for relaxation at those temperatures.⁸

To conclude, the present study constitutes, up to the authors knowledge, the first simulation carried out for a realistic model of a glass former having an internal degree of freedom of frequencies comparable with those of the ‘‘cage.’’ As shown above, such a fact results in a strong coupling of intermolecular and intramolecular dynamics, which has measurable effects in most dynamic properties.

ACKNOWLEDGMENTS

The authors acknowledge the financial support of Grant No. PB95-0072-C03-02 of DGICYT/Spain. M.A.G. thanks the Institut Laue-Langevin for the concession of a CFR contract. We thank N. G. Almarza for stimulating discussions.

¹S.R. Elliot, *Physics of Amorphous Materials* (Longman, London, 1983).

²See W. Götze, in *Liquids, Freezing and the Glass Transition*, edited by J.P. Hansen *et al.* (North-Holland, Amsterdam, 1991).

³R. Schilling and T. Scheidsteger, *Phys. Rev. E* **56**, 2932 (1997).

⁴O. Haida, H. Suga, and S. Seki, *J. Chem. Thermodyn.* **9**, 1133 (1977).

⁵A. Srinivasan, F.J. Bermejo, A. de Andrés, J. Dawidowski, J. Zúñiga, and A. Criado, *Phys. Rev. B* **53**, 8172 (1996); R. Fayos, F.J. Bermejo, J. Dawidowski, H.E. Fischer, and M.A. González, *Phys. Rev. Lett.* **77**, 3823 (1996); F.J. Bermejo, A. Criado, R. Fayos, R. Fernández-Perea, H.E. Fischer, E. Suard, A. Guelylah, and J. Zúñiga, *Phys. Rev. B* **56**, 11 536 (1997).

⁶M.A. Ramos, S. Vieira, F.J. Bermejo, J. Dawidowski, H.E. Fis-

- cher, H. Schober, M.A. González, C.K. Loong, and D.L. Price, *Phys. Rev. Lett.* **78**, 82 (1997).
- ⁷C. Talón, M.A. Ramos, S. Vieira, G.J. Cuello, F.J. Bermejo, A. Criado, M.L. Senent, S.M. Bennington, H.E. Fischer, and H. Schober, *Phys. Rev. B* **58**, 745 (1998).
- ⁸M.A. Miller, M. Jiménez-Ruiz, and F.J. Bermejo, *Phys. Rev. B* **57**, 13 977 (1998); M. Jiménez-Ruiz, M.A. González, F.J. Bermejo, M.A. Miller, N.O. Birge, I. Cendoya, and A. Alegría, *ibid.* **59**, 9155 (1999).
- ⁹M. A. Gonzalez *et al.* (unpublished).
- ¹⁰See, e.g., W. Kob, and H.C. Andersen, *Phys. Rev. E* **51**, 4626 (1995); **52**, 4134 (1995), and references therein.
- ¹¹P. Sindzingre and M.L. Klein, *J. Chem. Phys.* **96**, 4681 (1992).
- ¹²J. Alonso, F.J. Bermejo, M. García-Hernández, J.L. Martínez, W.S. Howells, and A. Criado, *J. Chem. Phys.* **96**, 7696 (1992).
- ¹³K.L. Ngai and C.M. Roland, *J. Phys. Chem. B* **101**, 4437 (1997).
- ¹⁴W.L. Jorgensen, *J. Phys. Chem.* **90**, 1276 (1986).
- ¹⁵L. Saiz, J.A. Padró, and E. Guàrdia, *J. Phys. Chem. B* **101**, 78 (1997); Also L. Saiz, Ph.D. thesis, University of Barcelona, 1998.
- ¹⁶M.A. González, E. Enciso, F.J. Bermejo, and M. Bée, *J. Chem. Phys.* **110**, 8045 (1999).
- ¹⁷The temperature and pressure of the system were controlled using the algorithm described in H.J.C. Berendsen, J.P.M. Postma, W.F. van Gunsteren, A. DiNola, and J.R. Haak, *J. Chem. Phys.* **81**, 3684 (1984).
- ¹⁸The intermediate scattering functions were calculated using the *n*-Moldyn package [G.R. Kneller, V. Keiner, M. Kneller, and M. Schiller, *Comput. Phys. Commun.* **91**, 191 (1995)], which doesn't account for changes in the shape or dimension of the box during the simulation.
- ¹⁹M. P. Allen and D. J. Tildesley, *Computer Simulation of Liquids* (Oxford University Press, Oxford, 1987).
- ²⁰J.P. Ryckaert, *Mol. Phys.* **55**, 549 (1985).
- ²¹D.J. Adams, E.M. Adams, and G.J. Hills, *Mol. Phys.* **38**, 387 (1979).
- ²²L. Perera, U. Essmann, and M.L. Berkowitz, *J. Chem. Phys.* **102**, 450 (1995).
- ²³J. Barthel, K. Bachhuber, R. Buchner, and H. Hetzenauer, *Chem. Phys. Lett.* **165**, 369 (1990).
- ²⁴B. D. Smith and R. Srivastava, *Thermodynamic Data for Pure Compounds* (Elsevier, Amsterdam, 1985).
- ²⁵C.A. Angell, *Science* **267**, 1924 (1995); M.D. Ediger, C.A. Angell, and S.R. Nagel, *J. Phys. Chem.* **100**, 13 200 (1996).
- ²⁶T.F. Sun, C.A. Ten Seldam, P.J. Kortbeek, N.J. Trappeniers, and S.N. Biswas, *Phys. Chem. Liq.* **18**, 107 (1988).
- ²⁷H.E. Fischer, F.J. Bermejo, G.J. Cuello, M.T. Fernández-Díaz, J. Dawidowski, M.A. González, H. Schober, and M. Jiménez-Ruiz, *Phys. Rev. Lett.* **82**, 1193 (1999).
- ²⁸P.G. Jönsson, *Acta Crystallogr., Sect. B: Struct. Crystallogr. Cryst. Chem.* **32**, 232 (1976).
- ²⁹P.K. Dixon, L. Wu, S.R. Nagel, B.D. Williams, and J.P. Carini, *Phys. Rev. Lett.* **65**, 1108 (1990).
- ³⁰M. Haughney, M. Ferrario, and I.R. McDonald, *J. Phys. Chem.* **91**, 4934 (1987).
- ³¹A.H. Narten and A. Habenschuss, *J. Chem. Phys.* **80**, 3387 (1984).
- ³²D.G. Montague, I.P. Gibson, and J.C. Dore, *Mol. Phys.* **47**, 1405 (1982).
- ³³S. Sarkar and R.N. Joarder, *J. Chem. Phys.* **100**, 5118 (1994).
- ³⁴M.M. Hoffmann and M.S. Conradi, *J. Phys. Chem. B* **102**, 263 (1998).
- ³⁵N. Asahi and Y. Nakamura, *J. Chem. Phys.* **109**, 9879 (1998).
- ³⁶M. Matsumoto and K.E. Gubbins, *J. Chem. Phys.* **93**, 1981 (1990).
- ³⁷N. Karger, T. Vardag, and H.-D. Lüdemann, *J. Chem. Phys.* **93**, 3437 (1990).
- ³⁸R.-J. Roe, *J. Chem. Phys.* **100**, 1610 (1994).
- ³⁹F.H. Stillinger, *Science* **267**, 1935 (1995).
- ⁴⁰J.N. Roux, J.-L. Barrat, and J.-P. Hansen, *J. Phys.: Condens. Matter* **1**, 7171 (1989).
- ⁴¹J. Horbach, W. Kob, K. Binder, and C.A. Angell, *Phys. Rev. E* **54**, 5897 (1996).
- ⁴²R. Ludwig, M.D. Zeidler, and T.C. Farrar, *Z. Phys. Chem. (Munich)* **189**, 19 (1995).
- ⁴³S.W. Lovesey, *Theory of Neutron Scattering from Condensed Matter* (Oxford Science Publications, Oxford, 1986), p. 191.
- ⁴⁴M. Foret, B. Hehlen, G. Taillades, E. Courtens, R. Vacher, H. Casalta, and B. Dorner, *Phys. Rev. Lett.* **81**, 2100 (1998); F.J. Bermejo, M. García-Hernández, T. Mason, J.L. Martínez, E. Enciso, and A. Criado, *Phys. Rev. B* **50**, 13 286 (1994).
- ⁴⁵A. Criado *et al.* (unpublished).
- ⁴⁶F. Sciortino, P. Gallo, P. Tartaglia, and S.-H. Chen, *Phys. Rev. E* **54**, 6331 (1996); F. Sciortino, L. Fabbian, S.-H. Chen, and P. Tartaglia, *ibid.* **56**, 5397 (1997).